PHYSICAL REVIEW B VOLUME 44, NUMBER 6 1 AUGUST 1991-II

Structural characterization of nanometer-sized crystalline Pd by x-ray-diffraction techniques

M. R. Fitzsimmons*
Sektion Physik der Universität München, München, Federal Republic of Germany

J. A. Eastman
Argonne National Laboratory, Materials Science Division, Argonne, Illinois 60439

M. Müller-Stach and G. Wallner
Sektion Physik der Universität München, München, Federal Republic of Germany
(Received 17 December 1990)

Quantitative x-ray-diffraction measurements of ultrafine-grained (nanocrystalline) Pd samples and a coarse-grained polycrystalline reference foil were obtained using synchrotron radiation. The intensity profiles of the Bragg reflections from the nanocrystalline samples were considerably better represented by Lorentzian functions than by Gaussian functions, indicating that a large fraction of intensity from the Bragg peaks was found in the tails of the reflections. The remaining intensity differed only slightly for different grain-sized materials, therefore, atomic relaxations in the vicinity of grain boundaries in nanocrystalline Pd must be small in magnitude and/or extremely localized. The results of the present work do not support the previously proposed existence of either a "gaslike" grain boundary phase, or large quantities of vacancies or voids within the grains of nanocrystalline Pd, which produce broadly distributed diffuse scattering. The broadening of the Bragg reflections was related to the small particle size of nanocrystalline Pd, and strain located in the grains and/or interfacial regions. Evidence was seen for anisotropic grain shapes preferentially elongated along the [111] direction. The Debye-Waller parameter of nanocrystalline Pd was observed to be larger than the literature value for coarse-grained Pd, which suggests larger displacements of the atoms from their ideal lattice locations in the nanocrystalline material than in the coarse-grained material.

I. INTRODUCTION

Ultrafine-grained materials (typically having grain sizes of 5–50 nm) formed by room-temperature pressing of gas-condensed metal or ceramic powders[1,2] have been the subject of investigation since Gleiter[3] proposed that novel properties could be obtained in these so-called nanocrystalline materials. A variety of interesting properties have recently been reported, including both enhanced plasticity,[4] and greatly improved sintering behavior[5] of nanocrystalline TiO_2, as well as increased microhardness of nanocrystalline Pd and Cu[6]. The magnitude and symmetry of atomic relaxations occurring in the vicinity of grain boundaries are expected to be important in determining the properties of nanocrystalline materials, because a large fraction of atoms in these materials are located within only a few atomic jumps of a boundary. A complete characterization of the microstructure, including a determination of internal strain and grain boundary structure, is required to understand these properties.

In an earlier investigation, Zhu, Birringer, Herr, and Gleiter[7] studied nanocrystalline α-Fe using large-angle x-ray-diffraction techniques. Based on a comparison of measured and calculated intensity profiles, Zhu *et al.* reported a large diffuse background intensity. It was proposed that this diffuse intensity could only be accounted for by the presence of an interfacial region lacking both short- and long-ranged order, i.e. a solid "gaslike" phase. Eastman and Thompson[8] later pointed out that large diffuse background intensities, e.g., Laue monotonic scattering, could also be generated by other sources, such as large numbers of vacancies within the grains of the sample, or by ordered atomic relaxations in the interface region. One important limitation of these earlier experiments was the lack of a direct comparison between the diffuse background intensities from nanocrystalline and coarse-grained samples. Because nanocrystalline samples contain significantly more interfacial material than coarse-grained samples, a comparison of the powder-diffraction patterns from these samples should provide information about the diffuse scattering produced by the interfacial material. The purpose of the present paper is to characterize the structure of nanocrystalline Pd by comparing Bragg-peak profiles and background intensities from nanocrystalline Pd with those of the coarse-grained material.

II. EXPERIMENTAL

A. Specimen preparation

Two nanocrystalline Pd samples, referred to as *A* and *B* in this paper, have been studied. Sample *A* was prepared by one of us (J.E.), and sample *B* was furnished by Professor H. Gleiter. The samples were manufactured using the technique suggested by Gleiter,[3] which involves the production of ultrafine powders by the gas condensation method.[1,2] Briefly, high-purity ($\sim$99.997%) Pd

 ©1991 The American Physical Society

wire was evaporated in 500 Pa of high-purity ($\sim$99.997%) He producing nanocrystalline Pd powder. The powder was then consolidated using a pressure of $\sim$1.4 GPa at ambient temperature. Except during the evaporation of the Pd wire, the entire manufacturing process took place under vacuum ($\sim 10^{-5}$ Pa) conditions. The consolidated samples were disks with diameters of $\sim$9 mm. The thicknesses of specimens *A* and *B* were 0.18 mm and 0.08 mm, respectively. The densities of the samples were estimated to be $(80\pm10)\%$ of the literature value (12.02 g/cm^3) (Ref. 9) by weighing the samples and calculating their volume. Archimedes' technique, which is more accurate than direct measurements, has also been used to estimate densities of other Pd samples produced under identical conditions. This technique has been found to consistently yield larger density values (typically 90% of the literature value) than the direct measurements.[10] The coarse-grained Pd reference sample used in this study was a 0.10-mm-thick 99.9975% pure foil, which was cut into a 9-mm-diameter disk.

B. X-Ray techniques

Powder x-ray-diffraction measurements of the Pd specimens were taken at the medium-resolution two-axis spectrometer, G3, at HASYLAB, Hamburg, Germany in reflection mode at room temperature. X-rays with a wavelength of $\lambda=0.92$ Å from the DORIS storage ring at DESY, operating in parasitic mode, were selected using a double bounce Ge(311) monochromator. The extinction depth of the fundamental radiation in Pd was calculated to be 16 μm,[11] which was less than a tenth of the thickness of the samples; therefore, the samples were sufficiently thick to either absorb or diffract nearly the entire incident beam. The divergence of the monochromated beam was adjusted to be less than 4 mrad, using slits (S_1 and S_2 in Fig. 1) placed before and after the monochromator. The slits reduced the x-ray illumination to an area smaller than the size of the specimen; thus, background scattering from sources other than the sample were minimized. The incident intensity was monitored by deflecting a portion of the beam into a scintillation counter (*M* in Fig. 1) with a Kapton foil. Measurements of the diffracted radiation from the specimen (*S* in Fig. 1) were normalized with this incident flux reading. The samples were attached to a polished Si(111) wafer with a small amount of oil, and placed onto a two-circle goniometer. The goniometer was adjusted so that the plane defined by the circular face of the Pd specimen made an angle, $\omega=15°$, with the incident beam. Scattered intensity from the sample was detected using a Ge energy dispersive counter (*D* in Fig. 1) having an energy window of $\sim$300 eV width centered about the fundamental radiation of 13.48 keV; thus, additional sources of background that modify the energy of x rays outside of this window, were not counted by the detector. A pair of 1-mm-wide Ta slits, S_3, were placed immediately in front of the detector, defining the resolution of the experiment, $\Delta q_{\parallel}$, in the direction parallel to the scattering vector, τ ($\tau=4\pi\sin\theta/\lambda$). The resolution of the experiment, $\Delta q_{\perp}$, within the plane that contains the motion of the detector

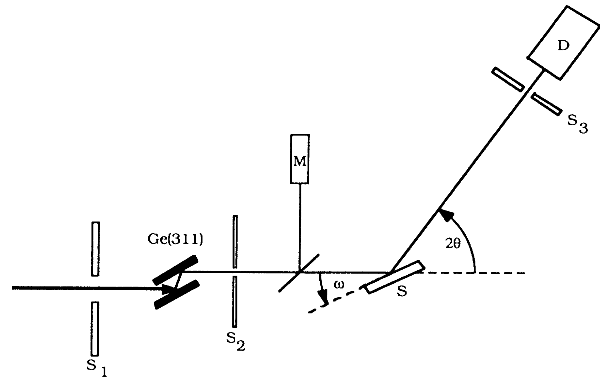

FIG. 1. Schematic diagram of the experimental setup at HASYLAB. Slits S_1 and S_2 define the dimensions and divergence of the incident beam before and after the double bounce Ge(311) monochromator. The incident beam is monitored by a scintillator counter *M*. Radiation scattered by the sample is detected by an energy dispersive detector *D*. A pair of slits, S_3, placed in front of the detector provided radial resolution to the experiment. Intensity measurements were obtained by fixing the angle ω between the incident beam and the specimen *S*, surface and scanning the detector in 2θ.

and orthogonal to τ, was partly determined by the divergence of the incident beam. The resolution out of the diffraction plane, Δq_{χ}, was limited by the size of the active area of the detector. The calculated lengths of $\Delta q_{\parallel}$, $\Delta q_{\perp}$, and Δq_{χ} for the scattering vector with magnitude $\tau=6$ Å^{-1} are 0.004 Å^{-1}, 0.024 Å^{-1}, and 0.2 Å^{-1}, respectively.

III. EXPERIMENTAL RESULTS

The intensity counted during either 10 or 20 s intervals was recorded as a function of scattering angle 2θ, and normalized to the incident beam intensity. Due to limitations of the software at the G3 beam line, the position of the sample remained fixed during the entire experiment and only the detector was moved, consequently, the orientation of the scattering vector changed during the execution of a 2θ scan. For a specimen containing preferred crystallographic orientations, i.e., texture, the integrated intensities and shapes of the Bragg reflections may be different than had the orientation of the scattering vector remained fixed, as is the case for a radial scan, where the orientation of the specimen is changed such that $\omega=\theta$. Because the grains of nanocrystalline Pd are extremely small and relatively free of texture, these specimens are expected to provide good isotropic measurements of the Bragg reflections. The Bragg reflections are also expected to be quite broad due to the small size of the nanocrystallites; therefore, the degradation of the instrumental resolution at large 2θ due to the asymmetric scanning geometry is not a serious limitation.

Using kinematical x-ray-diffraction theory,[12] the intensity measurements as a function of τ, $I(\tau)$, can be related

to the diffraction process, $S(\tau)$, from the sample by Eq. (1),

$$I(\tau)=I_0 LPA|f|^2 e^{-B_{298}\tau^2/8\pi^2} S(\tau) , \quad (1)$$

where I_0 represents a collection of physical constants. The Lorentz factor, $L(\theta)$, appropriate for this experiment is $(\sin\theta \sin 2\theta)^{-1}$. The polarization factor for a synchrotron beam from a double bounce monochromator is given by

$$P(\theta,\phi)=\frac{\pi^2+\sigma^2\cos^2 2\phi \cos^2 2\theta}{\pi^2+\sigma^2\cos^2 2\phi} , \quad (2)$$

where ϕ is the Bragg angle of the monochromator, and the polarization states, $\pi=0.9$ and $\sigma=0.1$, are the values for the synchrotron beam at HASYLAB. Since the synchrotron beam is primarily π polarized, $P(\theta,\phi)$ changes by only a few tenths of a percent over the entire range of 2θ. The absorption factor for a 2θ scan is related to ω and the mass absorption coefficient, $\mu=50.5\rho$ (cm^{-1}),[11] where ρ is the literature value of the density of Pd,[9] by Eq. (3):

$$A(2\theta,\omega)=\frac{\sin(2\theta-\omega)}{\sin(2\theta-\omega)+\sin\omega}\frac{1}{\mu} . \quad (3)$$

Another correction factor in Eq. (1) is the variation of the atomic form factor f, with scattering vector magnitude, and is given by Eq. (4):[11]

$$f(\sin\theta/\lambda)=\sum_{j=1}^{4} a_j \exp(-b_j \sin^2\theta/\lambda^2)+c+\Delta f'+i\Delta f'' . \quad (4)$$

The parameters a_j, b_j, and c are obtained from Ref. 11, and $\Delta f'$ and $\Delta f''$ are interpolated values of the dispersion factors for $\lambda=0.7107$ and 1.542 Å.[11]

The term $e^{-B_{298}\tau^2/8\pi^2}$ in Eq. (1) is the Debye-Waller factor of the material, which can be of thermal and/or static origin.[13] When the structure factor of the material is known, the value of B_{298} can be calculated by comparing the decay of the intensity of several reflections.

Identical correction factors were applied to the intensity data from the coarse-grained and nanocrystalline specimens. The corrected intensity data for the three specimens with $B_{298}=0$ are shown in Figs. 2(a), 2(b), and 2(c). The solid curves shown in the figures are fitted profiles from a model that is discussed later. Enlarged views of Figs. 2(b) and 2(c) containing the 400, 331, 420, 422, and 511/333 reflections are shown in Figs. 3(a) and 3(b) for nanocrystalline specimens A and B, respectively. The dashed line in Fig. 3(b) is the calculated profile for nanocrystalline specimen A, which exhibits much more peak broadening than specimen B.

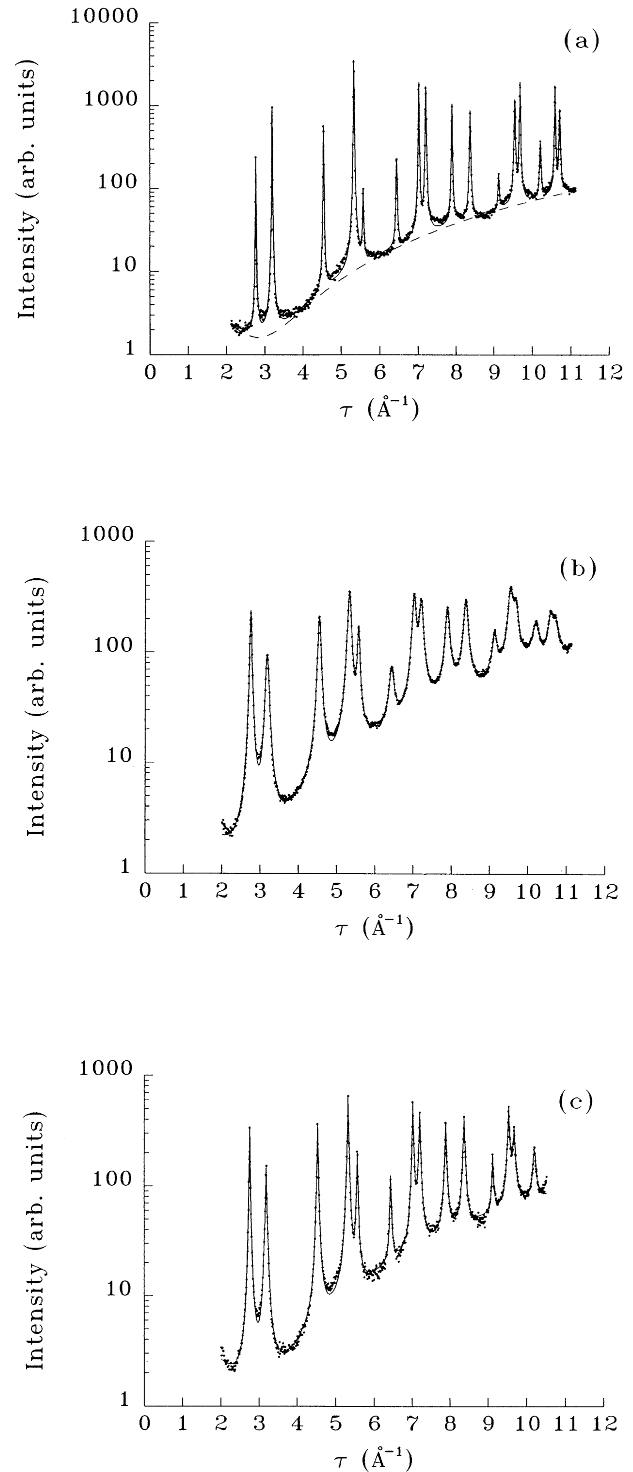

FIG. 2. Corrected intensity data from (a) a large grain-sized Pd control specimen, (b) nanocrystalline specimen A, and (c) nanocrystalline specimen B, plotted on a logarithmic scale vs scattering vector magnitude $\tau=4\pi\sin\theta/\lambda$. The solid line represents a least-squares fit of the data to the sum of 16 [25 in (c)] Lorentzian profiles and a quadratic polynomial intensity term. The quadratic polynomial used for the coarse-grained specimen is shown as the dashed line in Fig. 2(a).

IV. DISCUSSION

A. Data-fitting techniques

In order to obtain information about the shapes and integrated intensities of the Bragg reflections from coarse-

grained and nanocrystalline Pd, the intensity profiles in Fig. 2 were represented using the mathematical function given by Eq. (5), which is a combination of Lorentzian functions and a quadratic polynomial:

$$S(\tau)=\frac{1}{\tau}\sum_{i=i(hkl)}\left[\frac{\psi_i\Gamma_i/2}{(\Gamma_i/2)^2+(\tau-H_i)^2}\right]+d+e\tau+g\tau^2\ . \quad (5)$$

The parameters ψ_i, Γ_i, and H_i are the integrated intensity, full width at half maximum (FWHM), and position of the ith peak, respectively. The parameters of the quadratic polynomial are represented by d, e, and g in Eq. (5). For the coarse-grained specimen and nanocrystalline specimen A, the sum was taken over the 16 observed peaks.

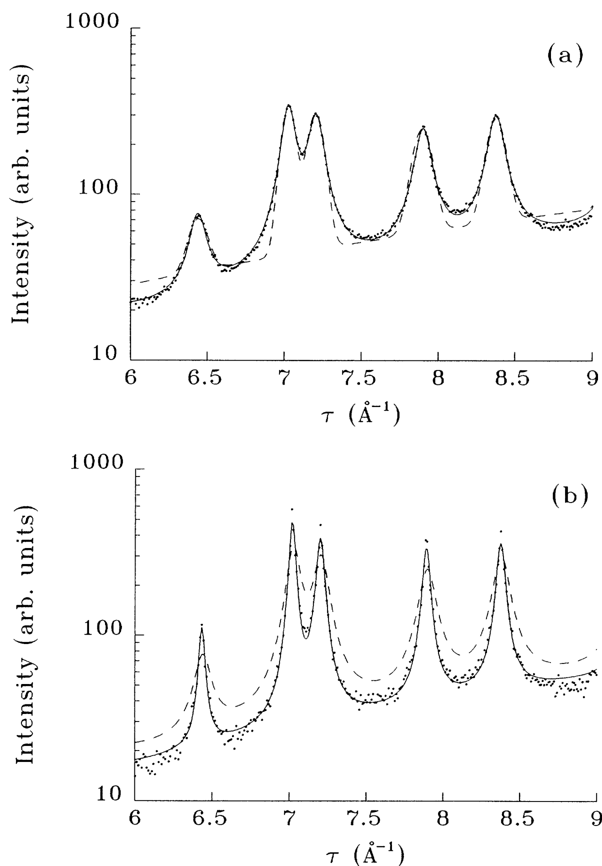

FIG. 3. An enlarged view of the 400, 331, 420, 422, and 511/333 reflections shown in Fig. 2 for (a) specimen A and (b) specimen B. The dashed line in (a) is the profile that best fits the data when Gaussian functions are used instead of Lorentzian functions. The solid line in (b) is the intensity profile that was calculated for nanocrystalline specimen B when only a single Lorentzian was used for each Bragg reflection from this specimen. The extra intensity at the maxima of the Bragg reflections in (b) can be explained by sharply peaked scattering from large crystallites in specimen B. The dashed line is the calculated profile from specimen A, which exhibits more peak broadening than specimen B.

The intensity data from specimen B could not be satisfactorily represented using a single Lorentzian curve for each Bragg peak. Such an attempt is shown as the solid line in Fig. 3(b). Two Lorentzians, one with a narrow FWHM and the other with a broad FWHM, for all but the 620 Bragg reflection from sample B gave a satisfactory fit to the data, and are shown as the solid line in Fig. 2(c). The intensity profile of the 620 Bragg reflection was too weak to justify more than one Lorentzian profile. The need for a pair of Lorentzians with different FWHM's centered at each Bragg reflection for specimen B can be explained by a bimodal grain-size distribution in this specimen. The existence of such a distribution is consistent with small-angle neutron scattering (SANS) observations of the specimen.[14] The narrow Lorentzian functions represent intensity diffracted from large coherent regions of the specimen, whereas, the broad Lorentzian functions correspond to intensity from the small-grained, i.e., nanocrystalline, regions of the specimen.

The set of parameters ψ_i, Γ_i, H_i, d, e, and g were calculated by simultaneously adjusting the parameters so as to minimize the value of χ_ν^2, which is a measure of error between the calculated profile and the intensity data containing over 800 measurements for each specimen. Values of $\chi_\nu^2 \sim 1$ were obtained for the fits to both sets of nanocrystalline data. A poorer value of $\chi_\nu^2=7$ was calculated for the coarse-grained specimen. Significant differences between the calculated and observed intensity profiles from this specimen occurred only near peak maxima. A pseudo-Voigt function, which is a weighted sum of a Gaussian function and a Lorentzian function, was also used to fit the data. From this analysis, the intensity profiles of the Bragg reflections from the coarse-grained specimen were somewhat better represented by a mixture of 93% Lorentzian-shaped intensity and 7% Gaussian-shaped intensity; however, the background intensity remained unchanged regardless of whether the Bragg peaks were purely Lorentzian shaped or contained a small amount of Gaussian-shaped intensity. Using the pseudo-Voigt analysis, the intensity peaks from the nanocrystalline specimens were found to be greater than 90% Lorentzian; therefore, the use of only Lorentzian functions in the analysis was justified, particularly since the total number of free parameters was reduced by 25%. Fits of the intensity data from the nanocrystalline specimens to Gaussian profiles were also attempted [such an attempt is shown as the dashed curve in Fig. 3(a)], but yielded values of χ_ν^2 in excess of 36, which is unacceptably large.

In principle, the parameters for the positions of the peaks, i.e., the H_i's can be related to one another by the lattice constant of the material; however, deviations of the peak positions of less than 0.2% from their expected locations were observed when the peak positions were independently optimized. These deviations could have been caused by small errors in the alignment of the instrument and specimen.[15] Alternatively, the positions of the Bragg reflections from a strained material may differ from those expected from an unstrained specimen.[13]

B. Background intensity comparisons

Because the Bragg reflections of the coarse-grained Pd specimen are so narrow, the regions between the reflections are good measurements of the experimental background from the specimen. The background intensity may include both diffuse scattering from the specimen and scattered intensity associated with the instrument, e.g., air scattering of the diffracted radiation. The dashed line shown in Fig. 2(a) is the intensity due to the quadratic polynomial in Eq. (5), and is a good representation of the background intensity from the coarse-grained specimen, particularly in the region where $\tau > 4$ Å^{-1}. The increase of the background intensity for $\tau < 4$ Å^{-1} is an artifact of the fitting procedure, because the quadratic polynomial does not correctly account for scattering from the beam path and sample surface, which are significant sources of scattering when 2θ is small.

Use of an intensity term of the form

$$d + e\tau + g[1 - \exp(-B_{298}\tau^2/8\pi^2)] ,$$

which includes an approximation for sources of background due to thermal diffuse scattering (TDS) (Ref. 15) instead of the quadratic polynomial, resulted in no significant change of the calculated profiles for any of the specimens. The lack of a significant change suggests that the quadratic polynomial is a suitable approximation to the TDS formulation for the range where intensity observations were made. While there exists physical rationale for using the TDS formulation to represent the background scattering from the coarse-grained specimen,[12] such rationale is lacking when the origin of diffuse scattering is largely from strain in the material caused by grain boundary defects.[13]

The intensity data from nanocrystalline specimen A, after the intensity of the Lorentzian-shaped Bragg peaks was removed, i.e., the intensity, which is not thought to be associated with the Bragg reflections, are shown in Fig. 4. In the case of the coarse-grained control specimen, this intensity can be called background intensity; however, the intensity in Fig. 4 may also include scattering due to the presence of a large volume fraction of interfacial material or voids in the nanocrystalline specimen. The solid line in Fig. 4 is the quadratic polynomial in Eq. (5) used for sample A, which represents the intensity not accounted for by the Lorentzian-shaped Bragg reflections. In the region where $\tau > 4$ Å^{-1}, the quadratic polynomial adequately predicts this scattering.

The solid, dashed, and dotted lines shown in Fig. 5 are the quadratic polynomial representations of the intensity not accounted for by the Bragg reflections from nanocrystalline specimens A and B, and the coarse-grained control specimen, respectively. In the region $\tau > 4$ Å^{-1}, where the polynomials are good representations of this intensity, there is no significant difference between the background scattering from the coarse-grained specimen and the non-Lorentzian scattering from specimen B. The non-Lorentzian intensity from nanocrystalline specimen A is $(8\pm8)\%$ larger than the background intensity measured from the coarse-grained control specimen in the region $4 < \tau < 11$ Å^{-1}.

Based upon a comparison of measured and computed interference functions of nanocrystalline α-Fe, Zhu *et al.*[7] found that random displacements of up to 50% of the nearest-neighbor spacing bcc Fe, $a_0/2\langle 111\rangle$, in a four plane grain boundary region comprising about half of the total sample volume, were required to account for the intensity observed between high-order Bragg reflections. If smaller, but still significant, random displacements of up to 15% of $a_0/2\langle 111\rangle$ in the grain boundary region were used in their model (see Fig. 4 of Ref. 7), then the intensity between the Bragg peaks was calculated to be only $\sim 50\%$ of the observed intensity. Eastman and Thompson[8] have shown that an increase of the background intensity can also be produced by other means, such as scattering from a large volume fraction of

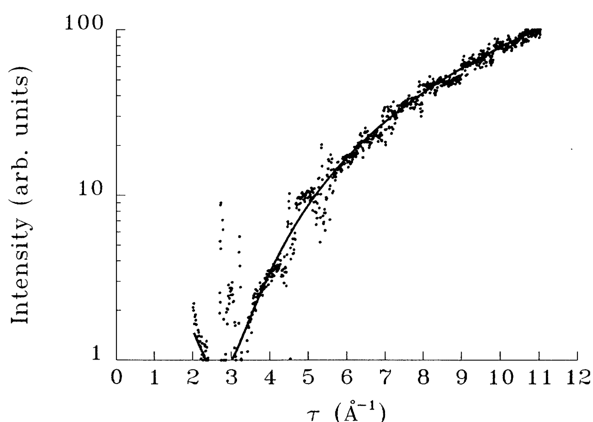

FIG. 4. The intensity not accounted for by the Lorentzian-shaped Bragg reflections from nanocrystalline specimen A. The solid line is the intensity contribution calculated from the quadratic polynomial that was used to obtain the intensity fit shown in Fig. 2(b).

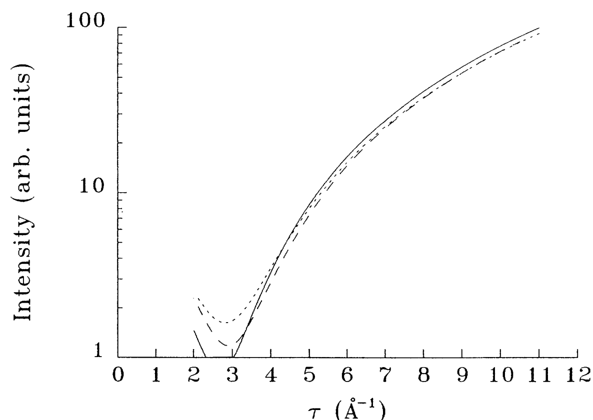

FIG. 5. The quadratic polynomials that were used to fit the intensity data from the coarse-grained specimen (dotted line), nanocrystalline specimen A (solid line), and B (dashed line). The quadratic polynomial for the coarse-grained specimen represents background intensity from thermal diffuse scattering and other sources of instrumental background.

vacancies and/or voids within the grains. An important limitation of both studies is that no direct experimental comparison was made between the diffuse background intensity from nanocrystalline and coarse-grained specimens.

A large increase of the background intensity similar to that observed by Zhu *et al.* was not seen from nanocrystalline Pd; rather, the intensity between the Bragg peaks was shown to be primarily intensity from the tails of neighboring Lorentzian-shaped intensity peaks. When the Lorentzian-shaped intensity was removed from the data, the remaining intensity was not significantly larger than the background intensity measured from the coarse-grained control specimen. This implies that atomic relaxations in the vicinity of grain boundaries in nanocrystalline Pd, and the strain contained within the grains of the material, contributed intensity to Lorentzian-shaped peaks located at or near the positions of Bragg reflections. In other words, the Lorentzian-shaped intensity peaks contain diffuse scattering from the grain boundary defects in nanocrystalline Pd. Because little, if any, broadly distributed diffuse scattering was observed from nanocrystalline Pd, the volume fraction of material that generates such intensity must be small and/or contain atomic relaxations of small magnitude.

A significant portion of the intensity between the Bragg peaks of nanocrystalline α-Fe may also belong to the tails of Lorentzian-shaped reflections. If the analysis by Zhu *et al.* assumed Gaussian-shaped Bragg-peak profiles, then the extent and magnitude of the atomic relaxations in the grain boundaries may have been overestimated. Of course, the structure of nanocrystalline α-Fe may be fundamentally different from that of nanocrystalline Pd, because of the different atomic structures of Fe (bcc) and Pd (fcc), and/or due to the greater affinity of Fe for impurities such as oxygen. In principle, the question as to whether these differences exist can be resolved by measuring the intensity profiles from impurity-free specimens of nanocrystalline and coarse-grained α-Fe with an instrument having a low and well characterized background.

C. Bragg-peak breadth analysis

Plots of the FWHM, $\Gamma(\tau)$, of the Lorentzian peaks from the coarse-grained (+), nanocrystalline specimen *A* (●), and the broad Lorentzian peaks from nanocrystalline specimen *B* (○) are shown in Fig. 6. Because the grain size ($\sim\mu$m) of the coarse-grained specimen is larger than the resolution of the synchrotron beam, and the amount of strain within the foil is expected to be small, a linear fit of the Bragg-peak widths from this specimen, Γ_c, to τ can be used to estimate the instrumental broadening $\Gamma_i(\tau)$. Such a fit is shown as the dashed line in Fig. 6. If the strain in the foil is not negligible, then $\Gamma_i(\tau)$ overestimates the actual of instrumental broadening. Because the width of a peak which is a sum of Lorentzian peaks is the sum of the widths from each of the peaks, the values of $\Gamma_A(\tau)$ and $\Gamma_B(\tau)$ for nanocrystalline specimens *A* and *B*, respectively, can be obtained by subtracting the instrumental broadening $\Gamma_i(\tau)$ from the

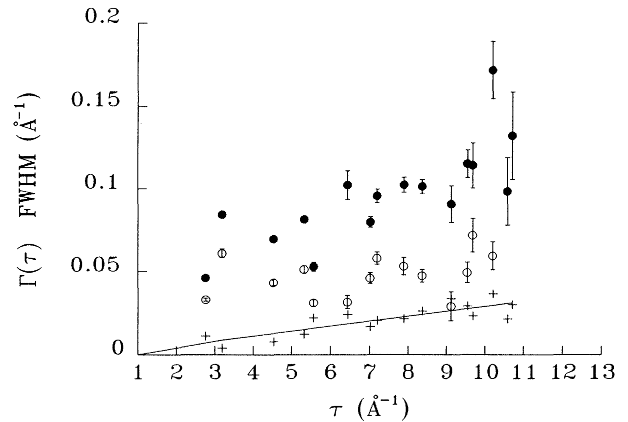

FIG. 6. The FWHM, $\Gamma(\tau)$, of the Lorentzian profiles from the coarse-grained specimen (+), nanocrystalline specimen *A* (●) and the broad reflections from nanocrystalline specimen *B* (○). The instrumental broadening, which is given by the solid line, has been removed from the nanocrystalline data.

values of Γ obtained from the fitted profiles for each reflection.

A Bragg reflection can be broadened by diffraction from small crystallites, and in some cases from defects within a material. Krivoglaz[13] has shown that if the amount of strain caused by a defect decays more slowly than $1/r^{3/2}$, where r is the distance from the defect, then the Bragg reflections from a material containing such a defect will be strain broadened.[13] A linear dislocation is one example of a defect that produces a region of strain that broadens Bragg reflections,[13] and is a major component of grain boundaries.[16]

The particle-size and strain components of broadened Bragg reflections from the same family represent a convolution of the profile associated with each component.[13] If the intensity profile due to strain contained in a nanocrystalline Pd is assumed to have a Lorentzian shape, then the broadening of the *hkl* Bragg reflection at τ, $\Gamma(\tau)$, is given by $2\pi/T_{hkl}+\tau\epsilon_{hkl}$, where T_{hkl} and ϵ_{hkl} represent the thickness and magnitude of strain, respectively, of the crystallites and interfacial regions in the $[hkl]$ direction.[17] This assumption is consistent with the observation that the measured intensity profile of a Bragg reflection is Lorentzian shaped. Such a profile can be produced by the convolution of a Lorentzian-shaped strain broadened profile with that of particle-size broadening, which is known to produce Lorentzian-shaped profiles.[17]

A list of T_{hkl} and ϵ_{hkl} for different pairs of reflections from nanocrystalline specimen *A* and the nonacrystalline portion of specimen *B* is shown in Table I. Because the intensity measurements were taken using an asymmetric diffraction geometry, the size and strain measurements for different reflections correspond to different crystallites in each specimen. If the specimens exhibit no texture, then the measurements listed in Table I would have been the same as those obtained from a symmetric diffraction

TABLE I. Particle sizes and strains for nanocrystalline Pd.

hkl pair	T_{hkl} (nm)	ϵ_{hkl} (10^{-3})	Specimen
111, 222	16±2	2.4±1.5	A
200, 400	9±2	6±4	A
220, 440	13±5	5±4	A
311, 622	20±17	12±5	A
111, 222	18±2	2±1	B
200, 400	7±1	-6±3	B
220, 440	11±3	0±4	B

geometry. From this table, the sizes of the crystallites in specimen A and the nanocrystalline portion of specimen B are seen to be nearly the same. The average grain sizes of 7–20 nm from the large-angle x-ray-diffraction measurements are larger than the values of (8±1) nm obtained from small-angle x-ray-scattering measurements of specimen A,[14] and (6±1) nm from transmission-electron-microscopy (TEM) measurements of similar samples. The difference may be due to an overestimate of the instrument broadening, which makes the Bragg-peak widths from the nanocrystalline specimens appear smaller than they actually are, thus, leading to an overestimate of the grain size.

The values of T_{hkl} are considerably anisotropic for both specimens, in fact $T_{h00} \sim T_{hh0}/\sqrt{2} \sim T_{hhh}/\sqrt{3}$. This anisotropy may be caused by a distribution of nanocrystallites with nonspherical shapes. High-resolution-electron-microscopy (HREM) studies of nanocrystalline Pd have shown that boundary faceting occurs, which could lead to anisotropic shapes.[18,19] From pictures of nanocrystalline Pd published in Ref. 18, the projection so the nanocrystallites onto the HREM micrographs are observed to be significantly noncircular. Kimoto[1] has reported observing anisotropic grain sizes of (1.7±0.3) nm parallel and (4.0±0.7) nm orthogonal to the ⟨111⟩ directions in uncompacted nanocrystalline Ag. Similar anisotropic behavior from uncompacted nanocrystalline Au (Refs. 1 and 20) and Ni (Ref. 1) specimens have also been reported. These observations, which were made from uncompacted nanocrystalline specimens, suggest that anisotropic shapes may be formed during the growth of the nanocrystalline powder in the inert atmosphere. Such growth may occur, if the [111] direction were an easy growth direction. In contrast to these measurements, Nieman and Weertman[10] have reported that the grains in compacted nanocrystalline Cu are equiaxed, using a Warren-Averbach analysis[12] of the shapes of ⟨h00⟩ and ⟨hhh⟩ type reflections.

An average strain of ~0.6%, which is calculated from the measurements reported in Table I for specimen A, is sufficiently large to suggest that plastic deformation of the specimen may have occurred during the compaction process.[9,16] Little, if any, strain broadening of the ⟨hh0⟩ and ⟨hhh⟩ type reflections was observed from the nanocrystalline portion of specimen B. The 200 reflection from this specimen was observed to be broader than the 400 reflection; thus, the slope of the line calculated from the widths of these reflections was negative. The negative slope may have been caused by a change of texture, to which a 2θ scan is sensitive. A narrowing of the 400 reflection compared to the 200 reflection was not observed from specimen A.

The much smaller amount of strain in the nanocrystalline portion of specimen B compared to that in specimen A may be due to a preferential deformation during compaction of large grains which were already present in the uncompacted powder from which specimen B was made. Alternatively, the lack of strain may be due to exaggerated grain growth during or subsequent to compaction, which could have taken place in order to relieve the strain in the nanocrystalline portion of specimen B.

Depending upon the concentration of defects, and the magnitude and range of the strain caused by the defects, the intensity distribution may be regarded as purely diffuse scattering that peaks at or near positions of Bragg reflections.[13] If the strain from grain boundaries in nanocrystalline Pd is of the type that produces such an intensity distribution, then the simple analysis of peak broadening used in the present work, and the application of some other techniques, such as the Warren-Averbach method,[13] to characterize particle shapes and strains in the material may be inaccurate. Perhaps, a better approach is to incorporate the distribution of crystallite sizes and shapes measured using TEM and/or small-angle-scattering (SAS) techniques into the calculation of the structure factor of a nanocrystalline material. Such a procedure may be able to accurately separate particle-size broadening from strain broadening of higher-order Bragg reflections, and to characterize the strain distortions in the material.

D. Debye-Waller factor determination

The logarithms of the integrated intensities of the Lorentzian peaks from specimen A (●) and the broad components of the Lorentzian peaks from specimen B (○) with their 2σ error bars are shown in Fig. 7 as a

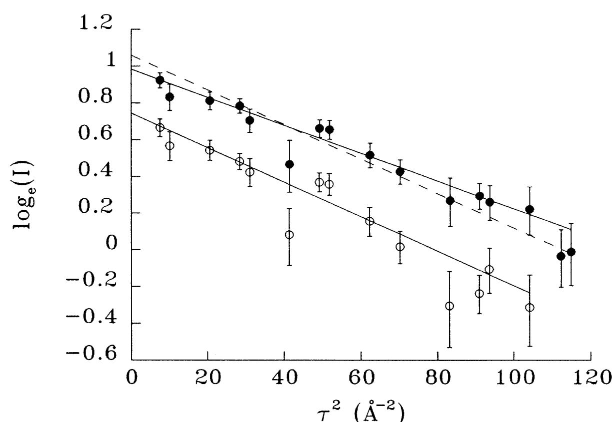

FIG. 7. The logarithms of the integrated intensities of the Lorentzian peaks from nanocrystalline specimen A (●) and the broad components of the Lorentzian peaks from nanocrystalline specimen B (○) vs τ^2. The solid lines are the lines which best fit the intensity data. The slopes of the lines are proportional to the Debye-Waller factors of the respective specimens. The dashed line is the line which best fits the intensity data from specimen A with the constraint of having the same slope as the line which best fits the intensity data from specimen B.

function of τ^2. With the exception of the two 400 Bragg reflections, the integrated intensities for each specimen exhibit Arrhenius relationships with τ^2, which are shown as the solid lines in Fig. 7. The scatter of the data about the lines can be partly attributed to a small amount of texture within the specimens. The dashed line in Fig. 7 is the best fit to the intensity data from specimen A with the constraint of being parallel to the line that best fits the intensity data from specimen B. The slope of the dashed line is inconsistent with the data from specimen A.

Using the slope of each solid line, the Debye-Waller parameter of the material, B_{298}, is calculated to be (0.60 ± 0.05) Å^2 for nanocrystalline specimen A, and (0.74 ± 0.06) Å^2 for the nanocrystalline portion of specimen B. Debye-Waller parameters calculated in this manner provide a measure of the distortion of atoms from their ideal lattice sites averaged over all crystallographic orientations and regions, i.e., interfacial and crystalline material, and may include distortions caused by both thermal motion and/or strain.[13] Since the crystallites in specimen A are similar in size to the nanocrystalline particles in specimen B, the significant difference between the Debye-Waller parameters of the two specimens may be related to the amount of strain within each specimen.

Krivoglaz[13] has shown that weakly distorted crystals, i.e., crystals containing strains that are short-ranged and generate small displacements of atoms, can be characterized by Bragg reflections which are not strain broadened, but whose integrated intensities are attenuated by a Debye-Waller factor that is related to the amount of distortion in the sample. On the other hand, the intensity peaks from a severely distorted specimen can be strain broadened, but their integrated intensities are the same as the integrated intensities of Bragg reflections from a specimen containing no distortion.[13] From the data shown in Figs. 6 and 7, specimen A is characterized by intensity peaks that are considerably more broadened and less attenuated than those from specimen B. These observations are consistent with the conclusion that specimen A is more severely distorted than specimen B. The striking fundamental differences between the distributions from the two specimens suggests that the microstructure of nanocrystalline Pd is very sensitive to the details of the manufacturing process.

An independent measurement of B_{298} for the coarse-grained specimen was not possible because this specimen was too textured to provide a meaningful value. The intensity measurements of the narrow component of the Lorentzian peaks from nanocrystalline specimen B also exhibited a large amount of texture. Lacking independent measurements, the nanocrystalline Debye-Waller measurements were compared to the literature value of (0.44 ± 0.03) Å^2 for the bulk material;[11] thus, the values of B_{298} for nanocrystalline specimens A and B are 36% and 68% larger, respectively, than the literature value for bulk Pd.

Increases of Debye-Waller parameters for nanocrystalline materials compared to their bulk values have also been reported elsewhere in the literature. Ohshima, Yatsuya and Harada[21] have reported a large Debye-Waller parameter of $B_{298}=1.18$ Å^2 from uncompacted nanocrystalline Pd with a 2 nm grain size. Their larger measurement of B_{298} compared to the values reported in the present work can be attributed to the smaller grain size of their material, and the presence of surface vibrational modes associated with uncompacted nanocrystalline specimens.[21] Harada, Yao, and Ichimiza[20] have also observed increases of B_{298} from uncompacted nanocrystalline specimens of Au. Using Mössbauer spectroscopy, Herr, Jing, Birringer, Gonser, and Gleiter[22] have reported a $\sim 78\%$ decrease of the Debye temperature of nanocrystalline Fe compared to the bulk material. This decrease can be related to an increase of the Debye-Waller parameter of the material. Rupp and Birringer[23] have also reported an increased heat capacity, which corresponds to an increase of B_{298}, of nanocrystalline Pd compared to that of coarse-grained Pd.

If the displacements of atoms from their ideal lattice sites are assumed to have cubic symmetry, which may not be true for displacements in grain boundary regions of the specimen,[24] then the rms displacement, $\langle u^2 \rangle^{1/2}$, of an atom in nanocrystalline Pd parallel to the scattering vector, can be calculated using the relation $\langle u^2 \rangle = B_{298}/8\pi^2$.[11] At room temperature, $\langle u^2 \rangle^{1/2}$ has a value of 2.7% of the nearest-neighbor spacing, $a_0/2\langle 110 \rangle$, in bulk Pd. Using the value of B_{298} obtained from specimen B, $\langle u^2 \rangle^{1/2}$ is calculated to be 4% of $a_0/2\langle 110 \rangle$ for nanocrystalline Pd. The structural model, which Zhu *et al.* proposed to explain the scattered intensity from nanocrystalline α-Fe, required displacements of atoms in the interfacial region on the order of 50% the nearest-neighbor spacing of bcc Fe. Such large displacements are clearly inconsistent with even the largest measurement of B_{298} for nanocrystalline Pd.

V. CONCLUSIONS

The scattered x-ray intensity from nanocrystalline Pd over a wide range of scattering vectors was well represented by a sum of Lorentzian-shaped peaks centered at Bragg reflections plus a quadratic polynomial. Because the Lorentzian peaks have long-ranged tails, a considerable fraction of the intensity between Bragg peaks is intensity from neighboring reflections. The intensity not accounted for by the Lorentzian peaks from both nanocrystalline specimens did not significantly differ from the background intensity measured from a coarse-grained control specimen; therefore, no evidence for a lack of short- or long-ranged order in grain boundaries, or the existence of appreciable quantities of vacancies or voids within the grains of nanocrystalline Pd that produce broadly distributed diffuse scattering, was observed.

The broadening of the intensity peaks from the nanocrystalline specimens has been related to particle-size and strain effects. Anisotropy of the particle shapes based on measurements of different families of Bragg reflections was observed from both nanocrystalline specimens. An average minimum particle size for the specimens was calculated to be ~ 8 nm in the $[h00]$ direction, and is in

reasonable agreement with SAS and TEM observations, while a larger average particle size of ~16 nm was obtained from measurements of ⟨*hhh*⟩ type reflections.

If the broadening of the Bragg reflections from nanocrystalline Pd is partly due to strain that produces Lorentzian-shaped intensity profiles, then strains of ~0.6% were calculated from the variation of the broadening of *hkl* Bragg reflections with τ from one specimen. Little strain broadening was observed from another nanocrystalline specimen. The lack of strain broadening from the second specimen was attributed to preferential deformation, or growth of large grains during compaction, which may have relieved the stress applied to the specimen by the compaction process.

The Debye-Waller parameter of one nanocrystalline Pd specimen was estimated to be at least 36% larger than the literature value for bulk Pd, while the Debye-Waller parameter from a second specimen was estimated to 68% larger than that of bulk Pd. The greater of the two estimates corresponds to a rms displacement of atoms from their ideal lattice sites on the order of 4% of the nearest-neighbor distance of fcc Pd.

Since the sizes of the nanocrystallites in the two specimens were observed by similar, the large difference between their Debye-Waller parameters was attributed to a difference in the amount of distortion within the specimens. The intensity peaks from the specimen with the larger Debye-Waller parameter were considerably less strain broadened than the peaks from the specimen with the smaller Debye-Waller factor. These fundamental differences suggest that the microstructure of compacted nanocrystalline Pd may be sensitive to the details of its manufacture.

ACKNOWLEDGMENTS

We wish to thank Professor J. Peisl for his encouragement of this project. We are grateful to Professor H. Gleiter and Dr. U. Herr for kindly providing us with nanocrystalline specimen *B*. The use of the facilities at the G3 beam line of HASYLAB are acknowledged. In particular, we thank Dr. R. Kirfel and Dr. A. Petkov for their help during the setup and execution of the experiment. One of us (M.F.) wishes to thank the American-German Fulbright Commission for providing financial assistance. J.E. was supported by the U.S. Department of Energy, BES-DMS, under Contract W-31-109-ENG-38. Additional funding was provided by the German Federal Ministry for Research and Technology (BMFT) under Contract Nos. 523-4003-03M23 and 03PE1LMU/2.

---

*Present address: Los Alamos National Laboratory, LANSCE, Los Alamos, NM 87545.

[1]K. Kimoto, J. Phys. Soc. Jpn. **8**, 762 (1953).

[2]K. Kimoto, Y. Kamilya, M. Nonoyama, and R. Uyeda, Jpn. J. Appl. Phys. **2**, 702 (1963).

[3]H. Gleiter, in *Deformation of Polycrystals: Mechanisms and Microstructures*, edited by N. Hansen *et al.* (Risø National Laboratory, Roskilde 1981), p. 15.

[4]H. Hahn, J. Logas, H. J. Höfler, and R. S. Averback, in *Superplasticity in Metals, Ceramics, and Intermetallics*, edited by M. J. Mayo, J. Wadsworth, M. Kobayashi, and A. K. Mukherjee, MRS Symposia Proceedings No. 196 (Materials Research Society, Pittsburgh, 1990), p. 71.

[5]H. Hahn, J. A. Eastman, and R. W. Siegel, Ceram. Trans. **B1**, 1115 (1988).

[6]G. W. Nieman, J. R. Weertman, and R. W. Siegel, Scr. Metall. **23**, 2013 (1989).

[7]X. Zhu, R. Birringer, U. Herr, and H. Gleiter, Phys. Rev. B **35**, 9085 (1987).

[8]J. A. Eastman and L. J. Thompson, in *Interfaces Between Polymers, Metals, and Ceramics*, edited by B. M. DeKoven, A. J. Gellman, and R. Rosenberg, MRS Symposia Proceedings No. 153 (Materials Research Society, Pittsburgh, 1989), p. 27.

[9]*CRC Handbook of Chemistry and Physics*, 70th ed., edited by R. C. Weast, D. R. Lide, M. J. Astle, and W. H. Beyer (CRC, Boca Raton, FL, 1989), p. B-27.

[10]G. W. Nieman and J. R. Weertman, *Proceedings of the Morris E. Fine Symposium, Detroit, 1990*, edited by P. K. Liaw *et al.* (The Minerals, Metals, and Materials Society, Warrendale, PA, 1991), pp. 243-250.

[11]*International Tables for X-Ray Crystallography III*, edited by C. H. Macgillavry and G. D. Rieck (Reidel, Dordrecht, 1983).

[12]B. E. Warren, *X-Ray Diffraction* (Dover, New York, 1990).

[13]M. A. Krivoglaz, *Theory of X-Ray and Thermal-Neutron Scattering by Real Crystals* (Plenum, New York, 1969).

[14]M. Müller-Stach, diplom thesis, 1990 (unpublished).

[15]H. P. Klug and L. E. Alexander, *X-Ray Diffraction Procedures* (Wiley, New York, 1974).

[16]C. R. Barrett, W. D. Nix, and A. S. Tetelman, *The Principles of Engineering Materials* (Prentice-Hall, Englewood Cliffs, NJ, 1973).

[17]H. Lipson and H. Steeple, *Interpretation of X-Ray Powder Diffraction Patterns* (St. Martin's, New York, 1970).

[18]G. J. Thomas, R. W. Siegel, and J. A. Eastman, Scr. Metall. **24**, 201 (1990).

[19]W. Wunderlich, Y. Ishida, and R. Maurer, Scr. Metall. **24**, 403 (1990).

[20]J. Harada, S. Yao, and A. Ichimiza, J. Phys. Soc. Jpn. **48**, 1625 (1980).

[21]K. Ohshima, S. Yatsuya, and J. Harada, J. Phys. Soc. Jpn. **50**, 3071 (1981).

[22]U. Herr, J. Jing, R. Birringer, U. Gonser, and H. Gleiter, Appl. Phys. Lett. **50**, 472 (1987).

[23]J. Rupp and R. Birringer, Phys. Rev. B **36**, 7888 (1987).

[24]M. R. Fitzsimmons, E. Burkel, and S. L. Sass, Phys. Rev. Lett. **61**, 2237 (1988).